

Nanoscale

Accepted Manuscript



This is an *Accepted Manuscript*, which has been through the Royal Society of Chemistry peer review process and has been accepted for publication.

Accepted Manuscripts are published online shortly after acceptance, before technical editing, formatting and proof reading. Using this free service, authors can make their results available to the community, in citable form, before we publish the edited article. We will replace this *Accepted Manuscript* with the edited and formatted *Advance Article* as soon as it is available.

You can find more information about *Accepted Manuscripts* in the [Information for Authors](#).

Please note that technical editing may introduce minor changes to the text and/or graphics, which may alter content. The journal's standard [Terms & Conditions](#) and the [Ethical guidelines](#) still apply. In no event shall the Royal Society of Chemistry be held responsible for any errors or omissions in this *Accepted Manuscript* or any consequences arising from the use of any information it contains.

1 Ultrafast direct fabrication of flexible substrate-supported designer 2 plasmonic nanoarrays

3 *Yaowu Hu^{1,3}, Prashant Kumar^{1,3,4}, Rong Xu², Kejie Zhao² and Gary J. Cheng^{1,2,3,*}*

4 ¹School of Industrial Engineering, Purdue University, West Lafayette, Indiana, USA-47907.

5 ²School of Mechanical Engineering, Purdue University, West Lafayette, Indiana, USA-47907.

6 ³Birck Nanotechnology Center, Purdue University, West Lafayette, Indiana, USA-47907.

7 ⁴Department of Physics, Indian Institute of Technology Patna, Bihta, India-801103.

8 9 10 **ABSTRACT**

11
12 Fabrication of plasmonic nanostructures have been an important topic for their potential
13 applications in photonic and optoelectronic devices. Among plasmonic materials, gold is one of
14 the most promising material due to its low ohmic loss at optical frequencies and high oxidation
15 resistance. However, there are two major bottlenecks for its industrial applications: 1) need for
16 large-scale fabrication technology for high-precision plasmonic nanostructures; and 2) need to
17 integrate the plasmonic nanostructures on various substrates. While conventional top-down
18 approaches involve high cost and low throughput, bottom-up approaches suffer from
19 irreproducibility and low precision. Herein, we report laser shock induced direct imprinting of
20 large-area plasmonic nanostructures from physical vapor deposited (PVD) gold thin film on
21 flexible commercial free-standing aluminum foil. Among the important characteristics of the
22 laser-shock direct imprinting are their unique capabilities to reproducibly deliver designer
23 plasmonic nanostructures with extreme precision and in ultrafast manner. Excellent size
24 tunability (from several μm down to 15 nm) has been achieved by varying mold dimensions and
25 laser parameters. The physical mechanism of the hybrid film imprinting is elaborated by finite
26 element modeling. Mechanical robustness test of the hybrid film validates a significantly
27 improved interfacial contact between gold arrays and underlying substrate. The strong optical
28 field enhancement was realized in the large-area fabricated engineered gold nanostructures. Low
29 concentration molecular sensing was investigated employing the fabricated structures as surface-
30 enhanced Raman scattering (SERS) substrates. The ability to ultrafast direct imprint plasmonic
31 nanoarrays on flexible substrate at multiscale is a critical step towards roll-to-roll manufacturing
32 of multi-functional devices which is poised to inspire several emerging applications.

33
34 **Keywords:** Multi-layer imprinting, Laser shock, Gold arrays, Flexible, Plasmonics, SERS.

35 *Corresponding author, E-mail: gjcheng@purdue.edu, Ph.: 765-494-5436.

36

1 1. Introduction

2 Designer gold arrays, representing ordered gold structures fabricated according to one's design,
3 have attracted tremendous interest due to the unprecedented ability in electromagnetic field
4 confinement and potential applications in a vast array of photonics and optoelectronics
5 technologies [1–3], ranging from chemical and biosensing [4–6] through to energy harvesting [7],
6 imaging [8,9], data storage [10–12] and optical tweezers for nanomaterials manipulation [13–16].
7 Gold is the most commonly used material in plasmonic and optical metamaterial devices due to
8 its chemical stability and small Ohmic losses at optical frequencies. While its use in basic
9 research keeps growing, the commercialization and practical implementations of laboratory
10 research to benefit the society have been greatly hindered by high cost and low throughput
11 inherited in current fabrication techniques [17–19]. For example, bottom-up approaches such as
12 guided growth and self-assembly suffer from poor control, reproducibility and scalability [20–
13 23]. Top-down techniques such as conventional lithography process [24–26] followed by
14 metallization and lift-off involve multiple steps and usually require high standard cleanrooms,
15 which need significant capital and energy investment. Furthermore, the conventional techniques
16 have exclusively been limited to flat surfaces. Exploring approaches to achieve gold arrays on
17 flexible substrates could bring advantages from their capability to wrap around non-planar
18 surfaces and combine with next generation flexible electronic devices with multiple functions.

19 Several methods have been developed to enable large-scale precise patterning in a relative rapid
20 and low-cost fashion. Using nanoimprint lithography [27–30] to mechanically deform
21 photoresists or polymers followed by curing at elevated temperatures or ultraviolet light
22 illumination has been a commonly employed approach; however, subsequent etching of residual
23 polymer, metal deposition and lift-off are still required steps to generate the final metallic arrays,

1 sophisticating the process. Template stripping [31–34] has been used to obtain smooth metallic
2 structures on flexible substrates over wafer-scale areas by thermal annealing of a polymer
3 substrate and a silicon mold with metal layers sandwiched in between, yet it lacks the capability
4 of roll-to-roll manufacturing. Thermoplastic forming of bulk metallic glasses [35,36] by taking
5 advantage of temperature dependence of material strength would generate geometrical
6 inaccuracies due to thermal expansion and capillary action. Consequently, the development of a
7 novel technique capable of high-throughput and precise direct fabrication of multiscale gold
8 arrays on flexible substrate is of great importance for next-generation devices and is expected to
9 be useful for various potential emerging applications.

10 In this article, we develop laser shock multi-layer imprinting (LSI) to realize ultrafast and precise
11 fabrication of flexible substrate-supported gold arrays. In this approach, the thin gold coating is
12 supported on a free-standing aluminum foil because of its availability at commercial scale and
13 good formability. Ultrahigh shock pressure is generated by laser ablation of graphite [37–39] to
14 deform the multi-layered film against a silicon mold. To gain insight of the underlying
15 phenomena in LSI of the hybrid, a finite element model (FEM) is developed to study the
16 transient stress and temperature fields. Structural integrity of the hybrid material system is tested
17 to evaluate its mechanical robustness. The capability of optical field confinement of the patterned
18 gold arrays are investigated by employing it as surface enhanced Raman scattering (SERS)
19 substrates for sensitive molecular detections.

20 **2. Materials and methods**

21 Fig. 1 (a) shows the silicon mold with various dimensions fabricated by electron-beam
22 lithography and dry/wet etching. The experimental set-up to achieve precision multiscale

1 patterned metallic structures by LSI is shown in Fig. 1(c). Q-switch Nd-YAG laser (Continuum®
2 Surelite III) (1064 nm wavelength and 5 ns pulse duration) was used to irradiate on a sacrificial
3 layer with graphite coating (Asbury Carbons, U.S.A.) sprayed on a 4- μm -thick Al foil (Lebow
4 Company USA). A fused silica was placed on top of the graphite coating to confine and enhance
5 plasma expansion. Intense laser fluence instantaneously evaporated the graphite layer and
6 ionized plasma and strong momentum was generated. The shock wave was then transferred onto
7 the target sample which sits directly on the fabricated micro-/nano- scale silicon mold. The
8 dimension of samples is around 10 mm \times 10 mm. The diameter of laser beam is controlled by a
9 focus lens and measured by using a photosensitive paper. The typically diameter used is 3 mm. A
10 motorized XY stage was used to achieve in-plane translation of the sample for laser scanning.
11 Deformation depths were closely monitored with the variation of single pulse laser intensity and
12 trench width. Trench mold of various trench widths from 4 μm and down to 15 nm were used in
13 the present experimental investigations. Laser intensities up to 0.7 GW/cm^2 (measured by using
14 Newport 1916c power meter) were applied to investigate laser shock imprinting of micro/nano
15 patterns. The target material is composed of a gold layer and a flexible substrate. In this study, a
16 4 μm thick aluminum foil was used as the flexible handling substrate. The foil was cleaned by
17 toluene, acetone, and Isopropyl alcohol successively for 5 minutes. After its natural dry, the
18 sample was mounted on a holder to coat a gold layer. The above mentioned laser shock
19 processing was applied to achieve micro/nano imprinting. The resultant imprinted film after peel
20 off from the micro/nano mold had inverted structures. Besides gold, other plasmonic materials
21 (such as silver or copper) which exhibit plastic formability under laser shock induced high-
22 strain-rate deformation could also be coated and processed. Au thin film of thickness 100 nm or
23 200 nm was deposited onto the flexible aluminum foil by electron beam deposition at a rate of 1

1 nm/s. An ultra-thin titanium layer (~5 nm) is used as adhesion layer. Al foil can be replaced by
2 flexible polymers as well, as the heat generated during nanosecond laser ablation is with small
3 dissipation length (within 500 nm) and it would thus not affect the substrate. The target film is
4 kept in dry environment and cut into smaller pieces for each usage. No future gold coating is
5 needed before its exhaustion.

6 The mechanical properties of laser shock processed hybrid film were evaluated from the
7 penetration force-displacement curves obtained from nanoindentation tests using a Keysight
8 Nano-Indenter G200 with a standard Berkovich diamond indenter. Three kinds of indentation
9 tests were performed during the experiment: indentations on the untreated, treated flat, treated
10 curve surface of the samples. To evaluate the mechanical properties along the thickness, tests
11 were performed under force control with several loading/unloading cycles. The loading time and
12 the hold period at maximum displacement was 10 s and 2 s, respectively. Afterwards, the
13 indenter was withdrawn at the same rate as during the loading cycle. From these tests,
14 mechanical properties like hardness and elastic modulus can directly be obtained from force-
15 displacement curves by standard Oliver and Pharr method [40].

16 A coupled temperature displacement dynamic FEM model was developed to simulate stress and
17 temperature fields. The analysis type was assigned to be plane strain. The element type used is
18 CPE4RT which features 4-node bilinear displacement and temperature, reduced integration and
19 hourglass control. Molecular dynamics simulation of indenter-structure interaction is carried out
20 to illustrate the influence of interfacial discontinuities on integrated mechanical response of the
21 hybrid film. An embedded atom method (EAM) potential with improved force matching
22 methodology [41] and FCC (face-centered cubic) structures were used for gold and aluminum. A
23 constant force of 0.05 eV/Å was applied to the indenter. Lennard Jones (LJ) potential was used

1 to describe the van der Waals interaction between gold and the mold. The calculation was in
2 microcanonical (NVE) ensemble around 300 K. The time step was 1 fs. Molecular detection
3 capability was demonstrated by soaking the fabricated sample in diluted rhodamine 6G aqueous
4 solution for 30 min followed by thoroughly cleaning with de-ionized water. Raman instruments
5 with laser wavelengths of 633 nm and power 0.25 mW were used to record Raman fingerprints
6 of molecules.

7 **3. Results and discussion**

8 Micro- and nanometer scale gold patterns are fabricated precisely and reproducibly, as shown in
9 the FESEM images in Fig. 1(d). The present LSI technique is equipped with the capability of
10 precision nanoscale imprinting of functional nanostructures on flexible substrates in scalable and
11 reproducible manner. Structures including but not limited to trenches, circles, and holes with
12 dimensions as low as 20 nm have been obtained on the hybrid film by a single laser shock.
13 Deposition of a layer of Au on thin flexible substrate generally results in much rougher surfaces,
14 because of thermal stress and deformation associated with rapid non-uniform heating and cooling
15 effect during the deposition process, large initial roughness of the supporting substrate, and
16 wrinkles generated during sample cleaning and handling. As shown in Fig. 1 (b), the measured
17 surface height variation of the deposited gold film on aluminum foil is around 200 nm, which is
18 more than 10 times larger than the usual surface roughness reported for rigid substrates.
19 However, as gold surface is placed against atomically smooth silicon mold, upon laser shock
20 processing, the ultra-high shock pressure generated during plasma expansion instantaneously
21 flattens the gold surface, resulting in much smoother surface with the measured surface height
22 variation ~ 10 nm, which is 20 times better than that without laser processing and the surface
23 smoothness is comparable to the features attained on rigid silicon substrate. The flattening effect

1 arises from plastic flow of gold and underlying substrate under laser shock pressure. Thus, LSI
 2 exhibits superior performance as compared to other existing imprinting technologies, as far as
 3 surface smoothness of fabricated features is concerned.

4 The deformation depth of micro/nanoscale features attained by LSI process is observed to be
 5 closely related to laser intensity and geometrical parameters of the mold. For a fixed trench width,
 6 higher laser power used for the purpose of forming, results in deeper trenches. Strong laser
 7 power dependence of deformation depth is visualized from approximately three-fold rise in
 8 deformation depth when laser intensity is increased from 0.1 to 0.4 GW/cm². Apparently, there is
 9 a threshold of laser intensity, over which one attains good formability. Typically, nanoscale
 10 features require a larger laser pressure to be deformed conformally, compared to micro or
 11 millimeter scale features. To ensure a high fidelity feature transfer for all structures with a single
 12 laser shock, a intensity of 0.7 GW/cm² is thus used.

13 **3.1 Deformation Mechanism of gold arrays by LSI**

14 To gain insight of the hybrid film shock forming process, a simplified model implemented by
 15 FEM is developed to illustrate stress and temperature fields with the advance of time.

16 **Table 1:** Mechanical and thermal properties of aluminum and gold [42,43]

| | Al | Au |
|---|-----------|-----------|
| Density (g/cm³) | 2.7 | 19.3 |
| Young's modulus (GPa) | 36 | 79 |
| Poisson ratio | 0.33 | 0.42 |
| Thermal conductivity (Wm⁻¹K⁻¹) | 237 | 318 |
| Specific heat capacity (J/g^oC) | 0.90 | 0.16 |

| | | |
|--|-------------------------|-------------------------|
| Coefficient of thermal expansion (K⁻¹) | 14.2 x 10 ⁻⁶ | 23.1 x 10 ⁻⁶ |
| Melting temperature (°C) | 660 | 1064 |

1

2 A simplified model for laser induced shock momentum is given by[44–49],

$$3 \quad \frac{dL(t)}{dt} = \frac{2}{Z} P(t) \quad (1)$$

$$4 \quad I(t) = P(t) \frac{dL(t)}{dt} + \frac{3}{2\alpha} \frac{d}{dt} [P(t)L(t)] \quad (2)$$

5 where P(t) is the laser induced shock pressure at given instant, I(t) the effective laser intensity at
 6 time t, L(t) the thickness of the interface at time t. α is a constant to represent a fraction of
 7 internal energy related to pressure. Z is the shock impedance given by[50],

$$8 \quad \frac{2}{Z} = \frac{1}{Z_1} + \frac{1}{Z_2} \quad (3)$$

9 where Z₁ and Z₂ are the impedances for the target metal and the confining media, respectively.

10 Impulse imparted by shock waves raises momentum of metal thin film to a level which suffices
 11 for the 3D plastic deformation conformal to the micro/nano scale molds. Metals under extreme
 12 laser shock pressure, achieves excellent 3D micro/nano forming due to high strain rate exceeding
 13 10⁶ s⁻¹. Ultrafast laser based 3D micro/nano forming results in compactness in formed materials
 14 which strengthens them. Since strain rate varies over huge range within minute fraction of
 15 second, plastic strain σ would have significant strain rate dependence. Considering that Johnson-
 16 Cook (J-C) strain sensitive plasticity model applies to the present case, the slope of the flow
 17 stress curve is independently influenced by strain, dimensionless strain rate and local
 18 temperature achieved in constriction.

$$\sigma = (A + B\varepsilon^n) \left(1 + C \ln \frac{\dot{\varepsilon}}{\dot{\varepsilon}_0}\right) (1 - T^{*m}) \quad (4)$$

where ε is the plastic strain, $\dot{\varepsilon}$ is plastic strain rate, $\dot{\varepsilon}_0$ is the reference strain rate. A, B, and C are material constants. T^* is the homologous temperature defined by,

$$T^* = \frac{T - T_r}{T_m - T_r} \quad (5)$$

where T_r is the transition temperature and T_m is the temperature at which melting occurs.

Table 2: Parameters for Johnson-Cook plastic model [43,51,52] for Al and Au with average grain size around 80 nm.

| | A (MPa) | B (MPa) | C | n | T_r ($^{\circ}$ C) | m |
|----|---------|---------|-------|-------|-----------------------|-----|
| Al | 140 | 157 | 0.016 | 0.167 | 527 | 1.7 |
| Au | 120 | 243 | 0.056 | 0.147 | 23 | 0 |

Temperature rise during the high strain rate process is considered by setting inelastic heat fraction for plastic flow. The temperature dependence of yield stress is set to zero, as it was found that yield stress of gold does not vary with temperature at low temperature region.[52] Two different sets of thermal and mechanical properties are assigned to represent the deposited polycrystalline Au layer and aluminum. ABAQUS software has been used to numerically simulate the stress as well as temperature fields during the process.

Fig. 2 (a) shows the successive stages of hybrid film deformation under shock pressure. At abrupt geometrical changes, materials are subjected to severe strain fields due to stress

1 concentration. For different laser conditions, the calculated von Mises stress fields and cross
2 sections are different, as shown in Fig. 2 (b-c). Stress field in gold coating is generally larger
3 than that in aluminum because of its stronger strain-rate sensitivity (Table 2). At the upper corner
4 of the mold, Au layer directly bears the reaction force from the mold and flows into the trench.
5 The thickness of Au layer inside the trench is thus anticipated to be thicker than that outside (Fig.
6 2(c, e, g)). Depending on the stage of the deformation and laser intensity, Au layer can suspend
7 on the trench (Fig. 2 (b, d, f)) for low laser shock pressure, or touch the bottom (Fig. 2 (c, e, g))
8 for high laser shock pressure. The gold layer under high shock pressure is punched against ultra-
9 flat silicon mold, thus generating a replicated smooth surface. The simulated results in Fig. 2 (b-e)
10 qualitatively agree well with those from experiments (Fig. 2 (f-g)).

11 Fig. 2(h) shows the strain energy of the hybrid during and after laser shock loading. While the
12 pulse duration is only 5 ns, the first peak in strain energy is found to occur several nanosecond
13 later than the peak in laser intensity, resulted from the prolonged plasma-induced shock pressure
14 due to confining media and a time delay for elastic and plastic stress wave propagation. The
15 second peak, which is more obviously present in the case of high laser intensity, emerges when
16 the film impacts on the bottom of the mold and kinetic energy of the material transfers into strain
17 energy of the system. Similar phenomena are found for the interface force (Fig. 2(i)). The strain
18 energy, interface force and local temperature rise (Fig. 2(j)) are found to decay as plastic stress
19 wave propagates and reflects. The maximum temperature rise is around 100 K and 20 K for laser
20 intensity of 0.48 GW/cm^2 and 0.27 GW/cm^2 , respectively. Thermal energy is uniform inside the
21 thin gold layer and dissipates quickly due to the high thermal conductivities of the metals.
22 Depending on the material properties, maximum temperature which locally rises in the ultra-high
23 strain rate deforming process could be increased, due to competing effects of heat generation and

1 dissipation. It should be noted that accurate material properties and processing parameters are
2 often difficult to obtain, especially in the present case of non-equilibrium plasma shock induced
3 micro/nanoscale high-strain-rate deformation. However, the calculated results shown in Fig. 2
4 could be interpreted qualitatively and serve as estimations of temperature rise and deformation
5 profile.

6

7 **3.2 Mechanical robustness of metal-flexible substrate interfaces:**

8 Extreme laser pressure burst in confined geometries is poised to elevate local temperature at
9 sharp corners. However, since laser pulse does not last longer than a few nanoseconds, diffusion
10 of heat will be fast and hence laser shock processing provides a technological platform for
11 relatively cold nanoforming which will have immense capabilities. Unlike hot forming
12 techniques, LSI is a cold forming process which provides extremely high strain rate, resulting in
13 high formability of metals and ultrasoft nanoscale surface features. Metals pushed into the
14 mold cavity with laser shock pressure experiences severe plastic deformation and
15 nanocrystallization around the corner of the nanomolds, followed with dynamic crystallization in
16 the mold cavity. As a result, the mechanical properties of the imprinted metal are enhanced, as
17 shown in the hardness values obtained from nanoindentation (Fig. 3 (a)). As the hybrid film gets
18 deformed into 3D shapes, the surface profile, local stress-strain and temperature history would
19 greatly impact the surface hardness. Thus variations of surface hardness after shock pressure
20 were expected. It was also found that surface hardness of LSI samples increases with increasing
21 laser intensity, due to dislocation multiplication and strain hardening. Due to spatial variations of
22 material thickness, local temperatures and strain histories, the measured hardness at different

1 locations varies, as listed in Table 4. On the top of the structures, the hardness is found to be the
2 highest, followed by the bottom, and then the unstructured areas. This agrees with experimental
3 and simulated cross-section profiles in Fig. 2 (b-g), with a thicker gold layer inside the trench.
4 For all samples treated by LSI, the hardness has a decreasing trend as the tip indents into the
5 surface, due to strong surface effect of LSI and size effect during indenter-surface interaction
6 [53,54].

7 For gold nanoarrays supported on flexible substrates, sufficient interfacial strength is needed for
8 practical applications. Fig. 3 (b) shows the obtained cross-sections of the hybrid film before LSI.
9 The interface between Au and Al is distinct and loose before LSI, which might result in Au layer
10 peel-off when the hybrid foil is bent. After LSI, significant interface improvement is observed.
11 As shown in Fig. 3 (c), it is found that Au and Al atoms diffuse to the adjacent layers,
12 overcoming surface imperfections such as oxide layer, adsorbed molecules and contaminations.
13 In order to study the influence of shock pressure on the integrated mechanical properties of the
14 hybrid film, the load-displacement curves were monitored on these samples during
15 nanoindentation. As shown in Fig. 3(d) for the untreated sample, large discontinuities are
16 observed at loads between 0.2 mN and 0.4 mN, or at penetration depths between 50 nm to 150
17 nm, for all 50 randomly selected locations on films before LSI. The jumps of displacement
18 during indentation are between 45 nm to 140 nm. This sudden displacement jump, known as
19 "pop-in" effect, was previously observed during indenting single-crystalline metals,
20 semiconductors, and ionic crystals, and was believed to be the transition from pure elastic to
21 plastic deformation as a result of homogeneous defect generation [55–57]. However, as shown in
22 the surface morphology of the indented area (Fig. 3 (a)), the test generated a pyramid indent on
23 the surface with no observable surface cracks, eliminating the possibility of brittle failures. Large

1 plastic deformation before pop-in is also clearly shown from the differences of loading and
 2 unloading curves in Fig. 3 (d). Thus “pop-in” in the present study should be attributed to loose
 3 contact at the internal interface, grain boundary sliding of the multi-crystalline gold coating, and
 4 large surface roughness. As listed in Table 3, LSI could effectively diminish the probability of
 5 occurrence of “pop-in”. The displacement jump length is largely shortened by LSI. The
 6 occurrence depth and force are both decreased upon laser shock, indicating better layer-to-layer
 7 contacts and improved surface morphology. The suppression of pop-in effect is a clear evidence
 8 of enhancing mechanical properties by LSI. To address the influence of interfacial strength on
 9 indenter-multilayered film interaction, molecular dynamics simulations with and without an
 10 interface void was carried out as shown in Fig. 3 (e-h). By comparing Fig. 3 (f) and Fig. 3 (h),
 11 the triangular indenter under constant loading is found to have a higher velocity when it
 12 penetrates to the proximity of the interfacial discontinuities due to void-induced stress-
 13 redistribution and subsequent collapsing, giving rise to the experimentally observed load-
 14 displacement jump. LSI could effectively densify porous thin-films, facilitate interlayer atom
 15 diffusion and introduce enhanced integration of multi-layered structures, thus preventing the
 16 aforementioned “pop-in” on LSI treated samples and resulting in mechanically robust multi-
 17 layered thin films.

18 **Table 3:** Pop-in event probability, length of displacement jump, occurrence depth and force
 19 variations with laser intensity.

| Laser Intensity (GW/cm ²) | Probability of pop-in (%) | Length of displacement jump (nm) | Occurrence depth (nm) | Occurrence force (mN) |
|---------------------------------------|---------------------------|----------------------------------|-----------------------|-----------------------|
| 0 | 100 | 45 | 73 | 0.31 |
| 0.07 | 53 | 12 | 55 | 0.2 |
| 0.27 | 0 | 0 | NA | NA |

| | | | | |
|------|---|---|----|----|
| 0.48 | 0 | 0 | NA | NA |
|------|---|---|----|----|

1

2

Table 4: Calculated hardness values.

| Load (μN) | Hardness (GPa) | | | |
|------------------------|----------------|------|--------|-----------|
| | Flat | Top | Bottom | Untreated |
| 0.125 | 1.67 | 2.05 | 1.77 | 1.92 |
| 0.25 | 1.32 | 1.46 | 1.31 | 2.07 |
| 0.5 | 0.92 | 1.07 | 1.04 | 0.47 |

3

4 The idea behind coating functional plasmonic gold layer on the top of flexible aluminum layer
 5 was to take advantage of excellent formability of aluminum and at the same time it would
 6 minimize the product cost with a huge margin. Mechanical properties studied by nanoindentation
 7 experiments indicate excellent structural integrity of the hybrid as forming is carried out by laser
 8 shock pressure. High strain rate processing, excellent heat dissipation and interfacial interactions
 9 are held responsible for enhanced mechanical robustness of the formed nanoscale features which
 10 ultimately provides fidelity which is needed for precision nanomanufacturing.

11 3.3 Molecular sensing by fabricated hybrid SERS platform

12 Plasmonic gold coating when nanopatterned, bear significance due to their capability of focusing
 13 light at one's will. The structure dimensions of the generated pattern define the local electric
 14 field when light is incident upon them. LSI is spatially selective in ultrafast fabrication of
 15 multiscale designed patterns consisting of gold nanostructures, as shown in Fig. 4 (a-b). By
 16 adjusting the structural dimensions, different field enhancements could be generated (Fig. 4 (c-
 17 d)). In general, by reducing slit width of the nanostructures, higher field confinements could be

1 achieved according to our FDTD simulations in Fig. 4 (d). To experimentally demonstrate the
2 field enhancement capability, molecular sensing of 70 nM Rhodamine 6G (R6G) (Sigma Aldrich)
3 was tested. The laser power is kept low while spectral recording was carried out, to avoid
4 apparent temperature rise of the samples which possibly can photocarbonize R6G molecules.
5 The molecules are off resonance at 633 nm red laser excitation, so that the detected signals could
6 be attributed to field enhancement. As shown in Fig. 4 (e), under transverse magnetic (TM) mode
7 excitation, the luminescence background of Au is found to be hugely increased after laser shock
8 patterning of Au film into nanoscale trench. Vibrational fingerprints of the molecules at 613, 775,
9 1187, 1360, 1509 and 1650 cm^{-1} could clearly be distinguished when molecules are anchored by
10 Au trenches, which is of significant difference as compared to the background Raman spectrum
11 recorded for flat Au surface. Such distinctions of Raman peaks are due to local electric field
12 evolved under incident light. The optical field enhancements under laser illumination are also
13 shown in our FDTD simulations in Fig. 4 (f). Few/single molecule detection could be carried out
14 in future by designing more complex structures, optimizing the geometrical dimensions and
15 shifting the plasmonic resonance wavelength to the resonant frequency of molecules to be
16 diagnosed. For surface-enhanced Raman scattering (SERS) effect from an ordered array with
17 deterministic hot spots intensities and locations, our result is apparently higher than that reported
18 by Zhu et al.[58], where a much higher molecular concentration of R6G was used onto gold-void
19 nanostructures fabricated by self-assembly assisted electrochemical deposition process under
20 molecular resonance frequency. It should be noted that SERS effect in this study is a proof of
21 field enhancement capability of the orderly structured metal foil with functional coating. With
22 this capability, various applications based on light-matter interaction, such as nanophotonic

1 devices and circuits, energy conversion devices, imaging, surface enhanced Raman scattering,
2 and photothermal applications, could be pursued with proper structural design in the future.

3

4 Patterning of hybrid films by LSI is demonstrated to be facile, rapid, economic, scalable and
5 reproducible. Moreover, while most of bottom-up patterning techniques involve several steps
6 including chemical treatments, heat treatments etc; top-down approaches suffers reproducibility
7 issues and pose operational barrier for manufacturing of nanoscale features. LSI provides a
8 viable solution to such outstanding issues and is deemed to be potential futuristic technology for
9 precision manufacturing of functional nanoarchitectures. The present method exploits excellent
10 formability of aluminum metal and at the same time, gold surface coating provides plasmonic
11 functionality to the printed 3D nanoshapes. Gold coating on the top of aluminum foil can be
12 replaced by other functional materials and thus one can attain 3D nanoshapes of desirable
13 functional materials. The present experimental investigation thus gives birth to an innovative
14 technology, capable of catering desired 3D nanoshapes with high precision as well as
15 reproducibility in scalable manner and with desired functionality.

16 **4. Conclusion**

17 In conclusion, gold arrays on flexible aluminum substrate have successfully been fabricated by
18 laser induced shock pressure. Precise control over structural dimensions, ultrafast processing
19 (nanosecond processing time), capability of roll-to-roll mass production at economic cost and in
20 scalable manner are some of the attributes of this emerging technology. The multi-layered
21 deformation mechanism is investigated by developing a continuum model to study the induced
22 stress wave propagation and temperature rise. The hybrid film treated by LSI shows improved

1 surface smoothness, better interface and enhanced mechanical integrity for robust use. Patterned
2 gold nanostructures act as an excellent optical antenna and results in strong optical field
3 confinement, which have aptly been exploited for sensitive molecular detection. Cold processing
4 nature of LSI would suit to precision nanomanufacturing of functional structures on a variety of
5 flexible substrates and thereby would find bio-applications. Since LSI is material wise versatile,
6 it could provide ultrafast production of patterned functional nanofeatures laminated on flexible
7 substrates with resolution beyond the limitations set by beam diffraction or scattering in
8 conventional photolithography techniques, and has broad working window for various
9 dimensions.

10 **ACKNOWLEDGEMENTS**

11 The authors want to acknowledge the financial support from NSF CAREER Award (CMMI-
12 0547636), NSF Grant (CMMI 0928752) through the program of Materials Processing &
13 Manufacturing, Office of Naval Research Defense University Research Instrumentation Program
14 (DURIP), and Purdue Research Foundation research incentive award.

15

16 **REFERENCES**

- 17 [1] Ozbay E 2006 Plasmonics: merging photonics and electronics at nanoscale dimensions.
18 *Science***311** 189–93
- 19 [2] Schuller J a, Barnard E S, Cai W, Jun Y C, White J S and Brongersma M L 2010
20 Plasmonics for extreme light concentration and manipulation. *Nat. Mater.***9** 193–204

- 1 [3] Echtermeyer T J, Britnell L, Jasnos P K, Lombardo a, Gorbachev R V, Grigorenko a N,
2 Geim a K, Ferrari a C and Novoselov K S 2011 Strong plasmonic enhancement of
3 photovoltage in graphene. *Nat. Commun.***2** 458
- 4 [4] Qian C, Ni C, Yu W, Wu W, Mao H, Wang Y and Xu J 2011 Highly-ordered, 3D petal-
5 like array for surface-enhanced Raman scattering. *Small***7** 1800–6
- 6 [5] Henzie J, Lee M H and Odom T W 2007 Multiscale patterning of plasmonic
7 metamaterials. *Nat. Nanotechnol.***2** 549–54
- 8 [6] Lee S, Kumar P, Hu Y, Cheng G J and Irudayaraj J 2015 Graphene laminated gold
9 bipyramids as sensitive detection platforms for antibiotic molecules *Chem. Commun.*
- 10 [7] Hilali M M, Yang S, Miller M, Xu F, Banerjee S and Sreenivasan S V 2012 Enhanced
11 photocurrent in thin-film amorphous silicon solar cells via shape controlled three-
12 dimensional nanostructures. *Nanotechnology***23** 405203
- 13 [8] Zhang X and Liu Z 2008 Superlenses to overcome the diffraction limit. *Nat. Mater.***7** 435–
14 41
- 15 [9] Fang N, Lee H, Sun C and Zhang X 2005 Sub-diffraction-limited optical imaging with a
16 silver superlens. *Science***308** 534–7
- 17 [10] Mansuripur M, Zakharian a R, Lesuffleur a, Oh S-H H, Jones R J, Lindquist N C, Im H,
18 Kobayakov a and Moloney J V 2009 Plasmonic nano-structures for optical data storage.
19 *Opt. Express***17** 14001–14

- 1 [11] O'Connor D and Zayats A V 2010 Data storage: The third plasmonic revolution. *Nat.*
2 *Nanotechnol.***5** 482–3
- 3 [12] Pan L and Bogy D 2009 Data storage: Heat-assisted magnetic recording *Nat. Photonics***3**
4 2–3
- 5 [13] Wang K and Crozier K B 2012 Plasmonic trapping with a gold nanopillar.
6 *Chemphyschem***13** 2639–48
- 7 [14] Wang K, Schonbrun E, Steinvurzel P and Crozier K B 2011 Trapping and rotating
8 nanoparticles using a plasmonic nano-tweezer with an integrated heat sink. *Nat.*
9 *Commun.***2** 469
- 10 [15] Novotny L, Bian R and Xie X 1997 Theory of Nanometric Optical Tweezers *Phys. Rev.*
11 *Lett.***79** 645–8
- 12 [16] Roxworthy B J, Ko K D, Kumar A, Fung K H, Chow E K C, Liu G L, Fang N X and
13 Toussaint K C 2012 Application of plasmonic bowtie nanoantenna arrays for optical
14 trapping, stacking, and sorting. *Nano Lett.***12** 796–801
- 15 [17] Anon 2015 Commercializing plasmonics *Nat. Photonics***9** 477–477
- 16 [18] Ok J G, Seok Youn H, Kyu Kwak M, Lee K-T, Jae Shin Y, Jay Guo L, Greenwald A and
17 Liu Y 2012 Continuous and scalable fabrication of flexible metamaterial films via roll-to-
18 roll nanoimprint process for broadband plasmonic infrared filters *Appl. Phys. Lett.***101**
19 223102

- 1 [19] Varghese L T, Fan L, Xuan Y, Tansarawiput C, Kim S and Qi M 2013 Resistless
2 nanoimprinting in metal for plasmonic nanostructures. *Small***9** 3778–83
- 3 [20] Lee S, Hahm M G, Vajtai R, Hashim D P, Thurakitseree T, Chipara A C, Ajayan P M and
4 Hafner J H 2012 Utilizing 3D SERS active volumes in aligned carbon nanotube scaffold
5 substrates. *Adv. Mater.***24** 5261–6
- 6 [21] Lee S, Mayer K M and Hafner J H 2009 Improved localized surface plasmon resonance
7 immunoassay with gold bipyramid substrates *Anal. Chem.***81** 4450–5
- 8 [22] Blaaderen A Van, Ruel R and Wiltzius P 1997 Template-directed colloidal crystallization
9 *Nature* 321–4
- 10 [23] Trau M, Yao N, Kim E, Xia Y, Whitesides G and Aksay I 1997 Microscopic patterning of
11 orientated mesoscopic silica through guided growth *Nature***390** 674–6
- 12 [24] Rolland J P, Hagberg E C, Denison G M, Carter K R and De Simone J M 2004 High-
13 resolution soft lithography: enabling materials for nanotechnologies. *Angew. Chem. Int.*
14 *Ed. Engl.***43** 5796–9
- 15 [25] Zhang G, Zhang J, Xie G, Liu Z and Shao H 2006 Cicada wings: a stamp from nature for
16 nanoimprint lithography. *Small***2** 1440–3
- 17 [26] Kumar G, Tang H X and Schroers J 2009 Nanomoulding with amorphous metals.
18 *Nature***457** 868–72

- 1 [27] McAlpine M C, Friedman R S and Lieber C M 2003 Nanoimprint Lithography for Hybrid
2 Plastic Electronics *Nano Lett.***3** 443–5
- 3 [28] Chou S Y 1996 Nanoimprint lithography *J. Vac. Sci. Technol. B Microelectron. Nanom.*
4 *Struct.***14** 4129
- 5 [29] Lucas B D, Kim J-S, Chin C and Guo L J 2008 Nanoimprint Lithography Based Approach
6 for the Fabrication of Large-Area, Uniformly-Oriented Plasmonic Arrays *Adv. Mater.***20**
7 1129–34
- 8 [30] Guo L J 2007 Nanoimprint Lithography: Methods and Material Requirements *Adv.*
9 *Mater.***19** 495–513
- 10 [31] Zhu X, Zhang Y, Zhang J, Xu J, Ma Y, Li Z and Yu D 2010 Ultrafine and smooth full
11 metal nanostructures for plasmonics *Adv. Mater.***22** 4345–9
- 12 [32] Cherukulappurath S, Johnson T W, Lindquist N C and Oh S-H 2013 Template-stripped
13 asymmetric metallic pyramids for tunable plasmonic nanofocusing. *Nano Lett.***13** 5635–41
- 14 [33] Lee K L, Chen P W, Wu S H, Huang J Bin, Yang S Y and Wei P K 2012 Enhancing
15 surface plasmon detection using template-stripped gold nanoslit arrays on plastic films
16 *ACS Nano***6** 2931–9
- 17 [34] Nagpal P, Lindquist N C, Oh S-H and Norris D J 2009 UltrasMOOTH patterned metals for
18 plasmonics and metamaterials. *Science***325** 594–7

- 1 [35] Kumar G, Tang H X and Schroers J 2009 Nanomoulding with amorphous metals
2 *Nature***457** 868–72
- 3 [36] Liu X, Shao Y, Tang Y and Yao K-F 2014 Highly uniform and reproducible surface
4 enhanced Raman scattering on air-stable metallic glassy nanowire array. *Sci. Rep.***4** 5835
- 5 [37] Hu Y, Lee S, Kumar P, Nian Q, Wang W, Irudayaraj J J and Cheng G J 2015 Water
6 flattens graphene wrinkles: laser shock wrapping of graphene onto substrate-supported
7 crystalline plasmonic nanoparticle arrays *Nanoscale*
- 8 [38] Gao H, Hu Y, Xuan Y, Li J, Yang Y, Martinez R V., Li C, Luo J, Qi M and Cheng G J
9 2014 Large-scale nanoshaping of ultrasmooth 3D crystalline metallic structures *Science*
10 *(80-)*.
- 11 [39] Kumar P, Li J, Nian Q, Hu Y and Cheng G J 2013 Plasmonic tuning of silver nanowires
12 by laser shock induced lateral compression *Nanoscale*
- 13 [40] Oliver W C and Pharr G M 1992 An improved technique for determining hardness and
14 elastic modulus using load and displacement sensing indentation experiments *J. Mater.*
15 *Res.***7** 1564–83
- 16 [41] Ward L, Agrawal a, Flores K M and Windl W 2012 Rapid Production of Accurate
17 Embedded Atom Method Potentials for Metal Alloys *Model. Simul. Mater. Sci. Eng.*
- 18 [42] Li J, Gao H and Cheng G J 2010 Forming Limit and Fracture Mode of Microscale Laser
19 Dynamic Forming *J. Manuf. Sci. Eng.***132** 061005

- 1 [43] Pierazzo E, Artemieva N, Asphaug E, Baldwin E C, Cazamias J, Coker R, Collins G S,
2 Crawford D a., Davison T, Elbeshausen D, Holsapple K a., Housen K R, Korycansky D G
3 and Wünnemann K 2008 Validation of numerical codes for impact and explosion
4 cratering: Impacts on strengthless and metal targets *Meteorit. Planet. Sci.***43** 1917–38
- 5 [44] Fabbro R, Fournier J, Ballard P, Devaux D and Virmont J 1990 Physical study of laser-
6 produced plasma in confined geometry *J. Appl. Phys.***68** 775–84
- 7 [45] Gao H, Ye C and Cheng G J 2009 Deformation Behaviors and Critical Parameters in
8 Microscale Laser Dynamic Forming *J. Manuf. Sci. Eng.***131** 051011
- 9 [46] Liao Y, Suslov S, Ye C and Cheng G J 2012 The mechanisms of thermal engineered laser
10 shock peening for enhanced fatigue performance *Acta Mater.***60** 4997–5009
- 11 [47] Ye C, Suslov S, Lin D and Cheng G J 2012 Deformation-induced martensite and
12 nanotwins by cryogenic laser shock peening of AISI 304 stainless steel and the effects on
13 mechanical properties *Philos. Mag.***92** 1369–89
- 14 [48] Liao Y, Yang Y and Cheng G J 2012 Enhanced Laser Shock by an Active Liquid
15 Confinement—Hydrogen Peroxide *J. Manuf. Sci. Eng.***134** 034503
- 16 [49] Liao Y, Ye C, Gao H, Kim B-J, Suslov S, Stach E a. and Cheng G J 2011 Dislocation
17 pinning effects induced by nano-precipitates during warm laser shock peening:
18 Dislocation dynamic simulation and experiments *J. Appl. Phys.***110** 023518
- 19 [50] Gao H, Ye C and Cheng G J 2009 Deformation Behaviors and Critical Parameters in
20 Microscale Laser Dynamic Forming *J. Manuf. Sci. Eng.***131** 051011

- 1 [51] Jonnalagadda K, Karanjgaokar N, Chasiotis I, Chee J and Peroulis D 2010 Strain rate
2 sensitivity of nanocrystalline Au films at room temperature *Acta Mater.***58** 4674–84
- 3 [52] Karanjgaokar N J, Oh C S, Lambros J and Chasiotis I 2012 Inelastic deformation of
4 nanocrystalline Au thin films as a function of temperature and strain rate *Acta Mater.***60**
5 5352–61
- 6 [53] Zhang T, Xu W and Zhao M 2004 The role of plastic deformation of rough surfaces in the
7 size-dependent hardness *Acta Mater.* **52** 57–68
- 8 [54] Huang Y, Zhang F, Hwang K C, Nix W D, Pharr G M and Feng G 2006 A model of size
9 effects in nano-indentation *J. Mech. Phys. Solids***54** 1668–86
- 10 [55] Gouldstone a, Van Vliet K J and Suresh S 2001 Nanoindentation. Simulation of defect
11 nucleation in a crystal. *Nature***411** 656
- 12 [56] Lorenz D, Zeckzer a., Hilpert U, Grau P, Johansen H and Leipner H 2003 Pop-in effect as
13 homogeneous nucleation of dislocations during nanoindentation *Phys. Rev. B***67** 1–4
- 14 [57] Morris J R, Bei H, Pharr G M and George E P 2011 Size effects and stochastic behavior of
15 nanoindentation pop in *Phys. Rev. Lett.***106** 1–4
- 16 [58] Zhu X, Shi L, Schmidt M S, Boisen A, Hansen O, Zi J, Xiao S and Mortensen N A 2013
17 Enhanced light-matter interactions in graphene-covered gold nanovoid arrays. *Nano*
18 *Lett.***13** 4690–6
- 19

1

2

3 **Figure Captions:**

4 **Figure 1.** (a) Optical images of fabricated silicon mold. Scale bar: 1 mm. (b) Processing
5 procedures for patterning 3D structures on hybrid film: (1) initial film; (2) deposition of a thin
6 layer of functional material; (3) LSI process; (4) final film. Inserted are AFM images of gold
7 coated flexible foil before laser shock, flat and structured areas after laser shock respectively. (c)
8 Schematic drawing of LSI forming. (d) SEM images of obtained structures. Inserted is higher
9 resolution SEM image of nanostructure.

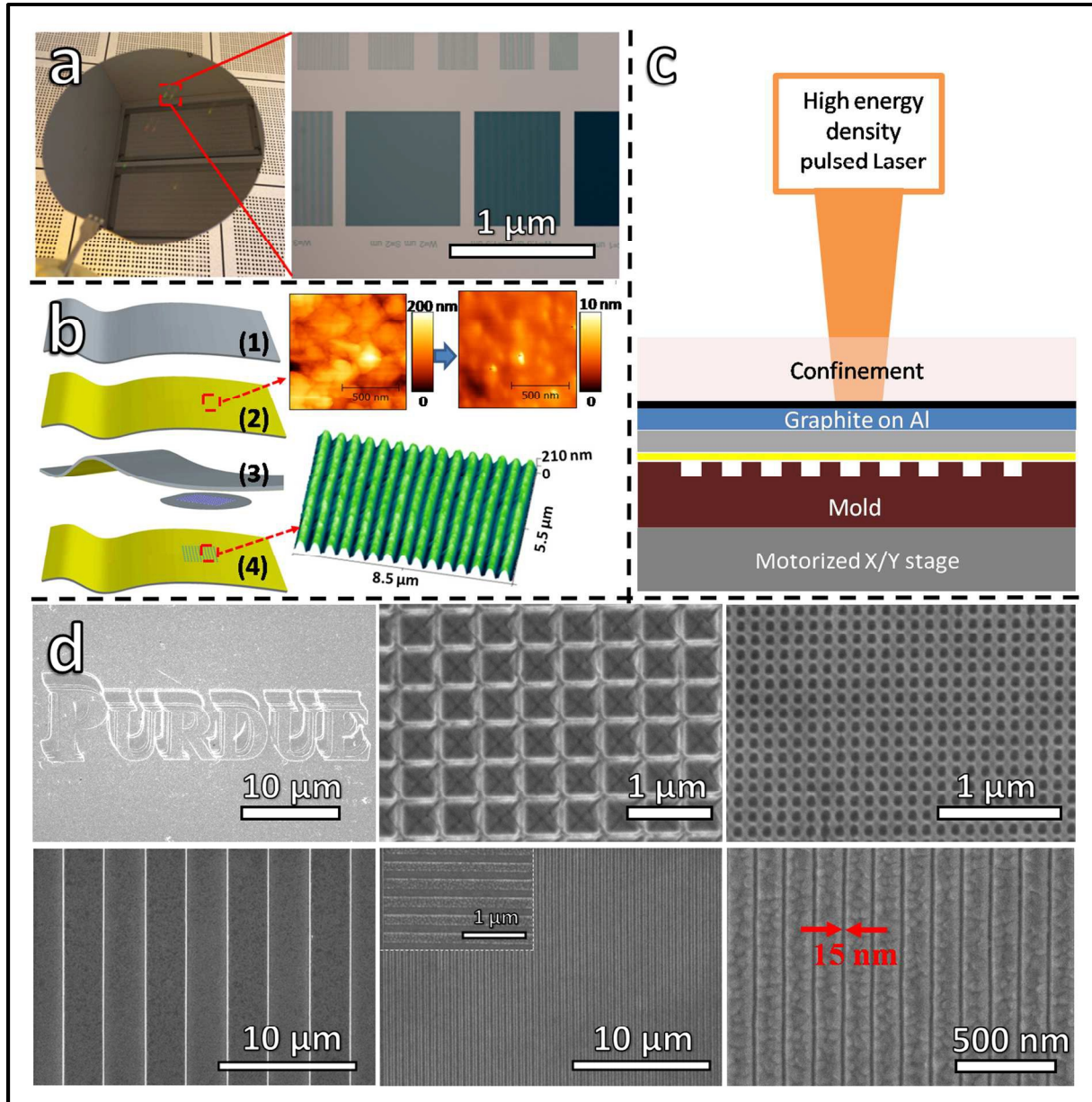
10 **Figure 2.** (a) Schematic of plastic strain generation during laser shock imprinting of hybrid films
11 with different mechanical properties: (1) initialization of plastic flow, (2) developed stage, (3)
12 final stage. Laser intensity: 0.48 GW/cm^2 . (b-e) Calculated von Mises stress fields (unit: MPa)
13 (b-c) and temperature fields (unit: K) (d-e) for laser intensities of 0.27 GW/cm^2 (b, d) and 0.48
14 GW/cm^2 (c, e), respectively. (f-g) Corresponding FESEM images of obtained cross-sections.
15 Scale bars: (a-e) 300 nm, (f-g) $1 \mu\text{m}$. (h) Strain Energy history of the system. (i) Corresponding
16 contact force at gold coating and aluminum film interface. (j) Temperature rise and dissipation
17 due to high strain rate deformation and thermal transport.

18 **Figure 3.** Enhanced mechanical properties by laser shock. (a) Experimental obtained hardness
19 values of untreated, shock imprinted samples with various laser intensities (LSI 1: 0.07 GW/cm^2 ,
20 LSI 2: 0.27 GW/cm^2 , LSI 3: 0.48 GW/cm^2 , loading force: 0.5 mN). Inset: typical AFM image of
21 indented surface. (b-c) FESEM imaging of surface morphologies for untreated samples (b)
22 showing sharp interface edges, and LSI treated samples (c). Scale bars: $1 \mu\text{m}$. (d) Load-
23 displacement curves obtained on samples before LSI treatment ("pop-in"), and at various
24 locations on generated structures after LSI. Laser intensity: 0.48 GW/cm^2 . (e-h) Schematic of
25 molecular dynamics simulations (e, g) and calculated velocity (z-direction, unit: $\text{\AA}/\text{fs}$) fields (f, h)
26 at 11 picosecond in nanoindentation of multi-layered films with (e-f) and without (g-h) interface
27 discontinuities. Scale bars (f, h): 4 nm.

28 **Figure 4.** Field confinement of fabricated flexible gold arrays. (a) Optical image of a circle with
29 nanostructures for LSI. Scale bar: $50 \mu\text{m}$. (b) Confocal Raman mapping of obtained circle
30 consisting of Au nanoarrays. Scale bar: $50 \mu\text{m}$. (c) FDTD simulations of trenches between two
31 slits with different slit width (100 nm, 50 nm and 30 nm). Structures are with depths of 50 nm
32 and with periods of 150 nm. Scale bars: 50 nm. (d) Line profiles of obtained field enhancements
33 in (c). (e) Raman spectra of R6G molecules on flat and patterned gold coated aluminum film,
34 inserted is the SEM image of the slit arrays (pitch: 150 nm; slit width: 15 nm; depth: 50 nm).
35 Scale bar: 150 nm. (f) Calculated local field under transverse magnetic (TM) mode and
36 transverse electric (TE) mode illuminations with incident light $\lambda = 633 \text{ nm}$ and mesh size 0.5 nm.
37 Scale bars: 50 nm.

38

1

2 **Figure 1.**

3

4

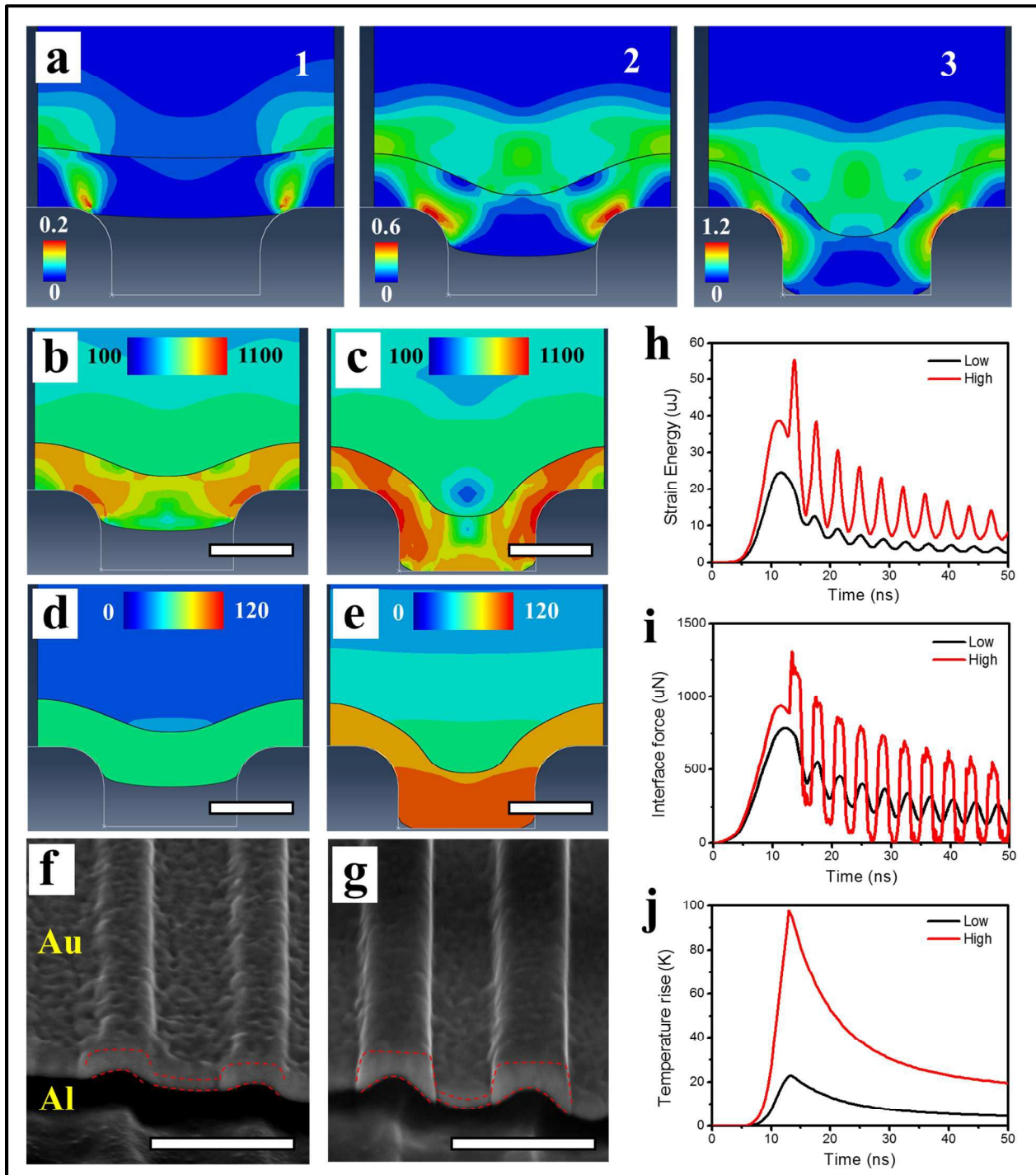
5

6

1

2 **Figure 2.**

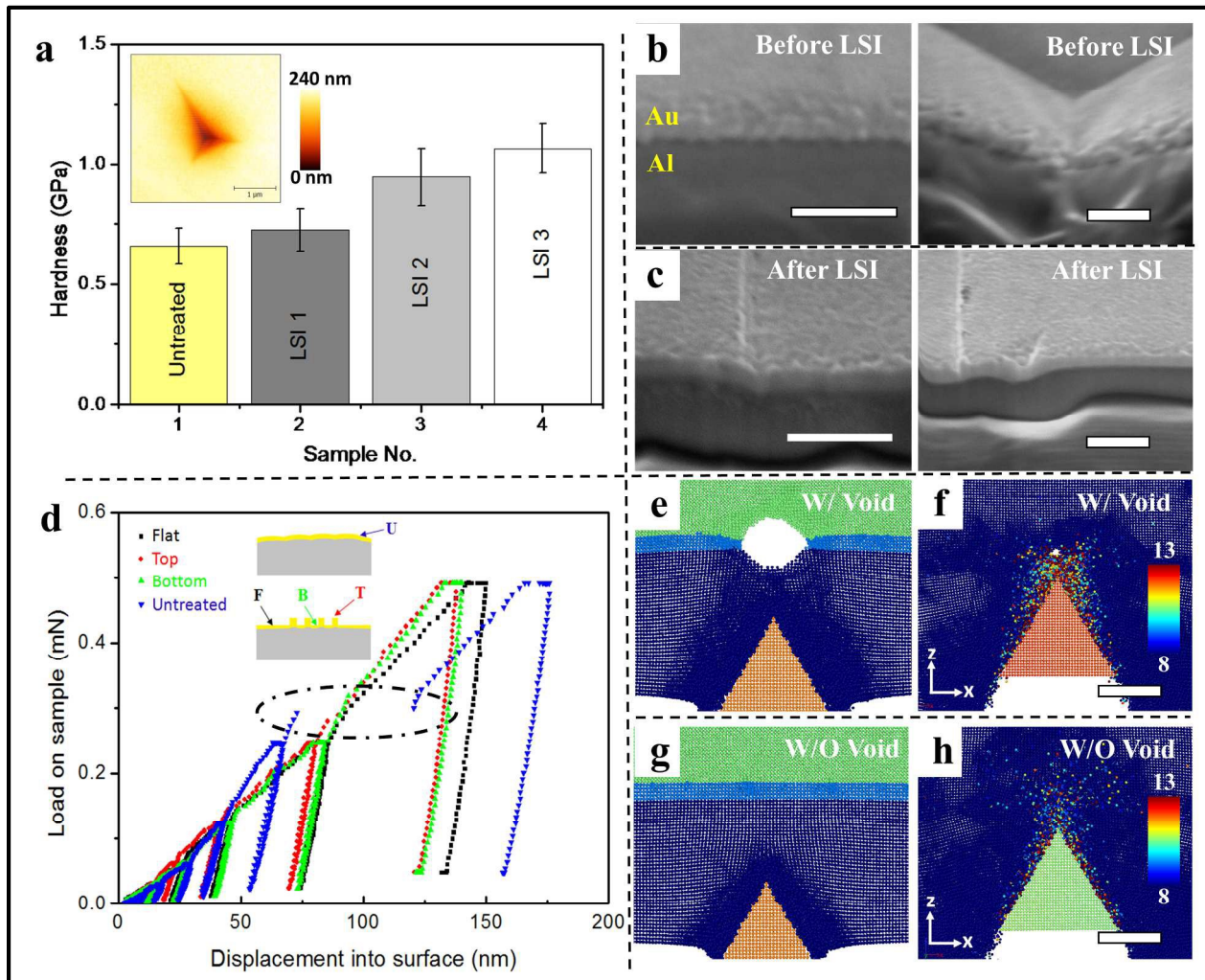
3



4

1

2

3 **Figure 3.**

4

5

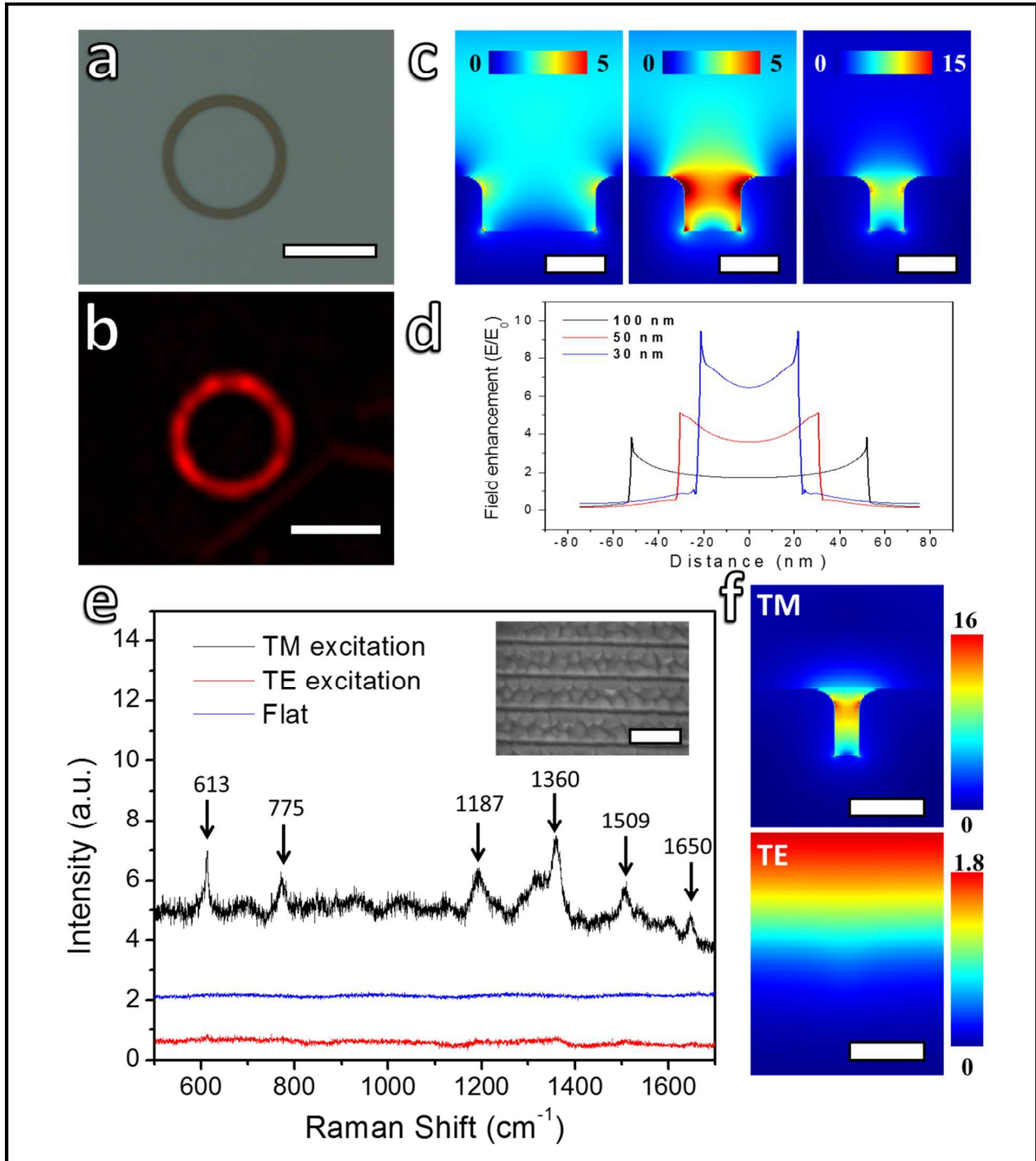
6

7

8

1

2

3 **Figure 4.**

4

1